HYBRID FUZZY LOGIC PROPORTIONAL PLUS CONVENTIONAL INTEGRATOR-DERIVATION CONTROLLER OF A NOVEL BDFIG FOR WIND ENERGY CONVERSION

Zoheir TIR
LEVRES-Research Laboratory, Department of Electrical Engineering
University of Eloued, B.P.789, 39000, El-Oued, Algeria,
E-mail: tir-zoheir@univ-eloued.dz

Rachid ABDESSEMED
LEB-Research Laboratory Department of Electrical Engineering,
University of Batna, 05000. Batna, Algeria.
E-mail: r.abdessemed@lycos.com

Abstract: *This paper discusses the control of a new topology of a brushless doubly-fed induction generator (BDFIG) using back-to-back PWM converters and its application to variable speed wind energy generation. The goal of BDFIG control is to achieve a similar dynamic performance to the doubly fed induction generator (DFIG), exploiting the well-known induction motor vector control philosophy. Here hybrid fuzzy logic proportional plus conventional integrator-derivation (Fuzzy P+ID) Controller for a BDFIG used in wind energy systems. The performance of Fuzzy P+ID has been investigated and compared with the conventional PID controller based BDFIG. The simulation results show that fuzzy P+ID controller is superior to PID controller under dynamic condition*

Key words: *Brushless doubly fed induction generator (BDFIG), power flow, PID controller, hybrid fuzzy logic proportional plus conventional integrator-derivation controller (fuzzy P+ID), wind energy system.*

1. Introduction

Over the last twenty years, the use of wind energy generation industry has been growing rapidly [1,2,3]. This is due to the fact that this energy source production of electricity is emission free [3,4,5]. Currently to the industry is heavily relying on the doubly fed induction generators (DFIG) for variable speed wind energy applications [1,3,6,7,8,9,10,11].
The use of the DFIG, however, increased the cost and complexity of the wind turbines [1,2,12,13,14]. The problems were caused by the configuration of the DFIG, which required a wound-type rotor and commutation brushes of the power transfer to or from the rotor windings [2,3,9,10,11,12,13,14]. These aspects created the need for frequent inspections and maintenance of the generator caused by the brushes wear and carbon accumulations on the internal components [1,2,14].
To overcome these disadvantages, a solution consists in using a brushless doubly fed induction generator (BDFIG) as shown in Fig. 1.

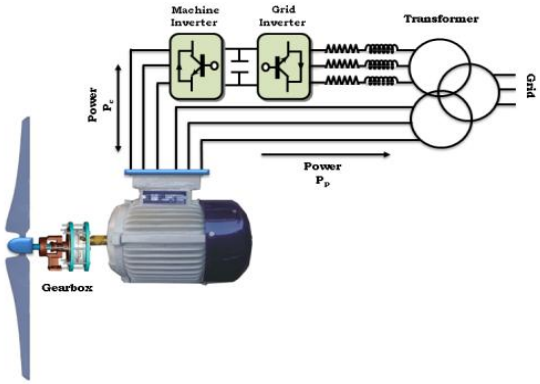

Fig. 1 BDFIG Configuration for Wind Power Generation

The basic structure of BDFIG is shown in Fig. 2. Two stator windings with different pole numbers (called power winding (PW) and control winding (CW)) and a special rotor winding. However, it allows putting a converter between the CW and the grid which is designed only for a part of the full power of the machine (about 30 %) [7,12,14,17,18,19]. By controlling correctly this converter, variable-speed operation is allowed and electrical power can be produced from the PW to the grid and also from the CW to the grid. Direct magnetic field coupling does not exist between the PW and CW, and the electromechanical energy conversion is realized by the magnetic field modulation of the rotor winding.

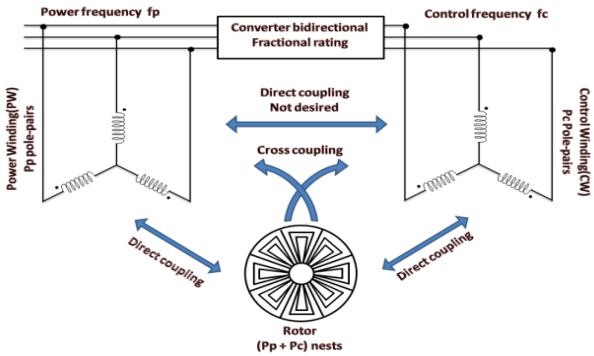

Fig.2 The basic structure of BDFIG

In order to assure the related cross-coupling effect by the simplest machine structure the number of rotor loops (Nr) has to be selected as [5,6,14,17,20]:

$$N_r = p_p + p_c \quad (1)$$

Direct coupling phenomena between the two stator windings must be prevented, so next supplementary restriction must be adopted [5,6,14,17,20]

$$p_p \neq p_c \quad (2)$$

In order to obtain the desired cross-coupling effect, the currents that both the PW and the CW induce at the rotor bars must evolve with the same frequency, [5,6,14,17,20]. The synchronous rotor speed is given by

$$\omega_r = \frac{\omega_p + \omega_c}{p_p + p_c} \quad (3)$$

Because of that a synchronization procedure is required in the start up phase. Once the synchronous operation mode is reached, the BDFIG shows a stable behaviour, and then the rotor speed can be easily controlled by ω_c [7].

The control law can be used in order to extract maximum power of the wind turbine for different wind speeds. In this paper presents a new hybrid control scheme to control a BDFIG. The proposed hybrid control scheme consists of a fuzzy logic proportional controller and a conventional integral and derivative controller (Fuzzy P+ID). In comparison with a conventional PID controller, only one additional parameter has to be adjusted to tune the Fuzzy P+ID controller [26,27,28,29,30]. The mathematical tool for the Fuzzy P+ID is the fuzzy set theory introduced by Zadeh [31,32,33].

This controller has the following features, [28].

1) Since it has only one additional parameter to be adjusted based on the original PID controller it is easy to design.

2) The Fuzzy P+ID controller keeps the simple structure of the PID controller. It is not necessary to modify any hardware parts of the original control system for implementation.

3) The sufficient stability condition shows that the same stability remains unchanged if the original PID controller is replaced by the Fuzzy P+ID controller [28].

Depending on the values of the average (steady state) wind speed, four zones may be identified in the static operation of BDFIG [2]. Zones I and VI, where the provided power is zero, are not concerned by this paper. The interest is here focused on zone II, called partial load zone, where the extracted power proportionally depends on the wind speed cubed, and the so called load zone (III), where the power must be limited to the nominal value.

This paper is organized as follows. Modeling of the wind generator and gearbox in Section 1, modeling of the BDFIG is provided in Section 2. BDFIG Controller Design is developed in Section 3. The synthesis controllers (PID, Fuzzy P+ID) are presented in Section 4. Finally, the system shown in Fig.1 is used for numerical simulation and the related results are presented.

2. Modeling of the wind turbine and gearbox

The theoretical power available in the wind is defined by Betz formula. It is given by

$$P_w = \frac{1}{2} \cdot \rho \cdot S \cdot v_w^3 \quad (4)$$

All this power is not recovered on the shaft of the turbine depending on the geometry of the turbine and frictions [2,4].

The effective efficiency conversion is given by the power coefficient (Cp), which is expressed by the following:

$$C_p = \frac{P_t}{P_w} \quad (5)$$

Where P_t is the mechanical power of the turbine and P_w is the available wind power.

The (per unit) speed or relative λ is the ratio between the linear blade speed and the speed of the wind.

$$\lambda = \frac{\Omega_t R}{v_w} \quad (6)$$

A typical relationship between C_p and λ is shown in Fig. 3. It is clear from this figure that there is a value of λ for which C_p is maximum and that maximize the power for a given wind speed. The peak power for each wind speed occurs at the point where C_p is maximized. To maximize the generated power, it is therefore desirable for the generator to have a power characteristic that will follow the maximum C_{p_max} line.

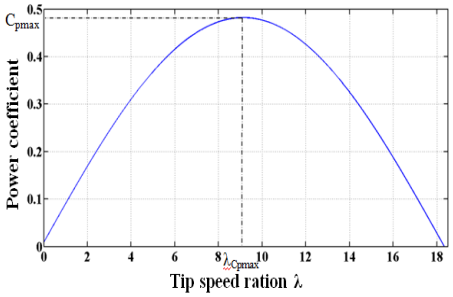

Fig. 3 The Power coefficient for the wind turbine model.

Taking into account equations (4), (5) and (6), power on the out axle of the turbine is then:

$$P_t = \frac{1}{2} . C_p . \rho . \pi . R^5 . \frac{\Omega_t}{\lambda^3} \quad (7)$$

Torque is then:

$$C_t = \frac{P_t}{\Omega_t} \quad (8)$$

$$C_{em} = \frac{P_t}{\Omega_t} = \frac{1}{2} \cdot \rho \cdot \pi \cdot R^3 \cdot C_p \cdot v_w^3 \quad (9)$$

With the multiplier of report/ratio G, the torque and speed become at shaft end;

$$C_g = \frac{C_t}{G} \text{ and } \Omega_t = \frac{\Omega_{mec}}{G} \quad (10)$$

When the turbine is coupled to a machine the mechanical equation at shaft end will be:

$$J\frac{d\Omega_{mec}}{dt} + f\Omega_{mec} = C_g - C_{em} \quad (11)$$

From these various equations the mathematical model of the turbine at shaft end is shown on Fig. 4.

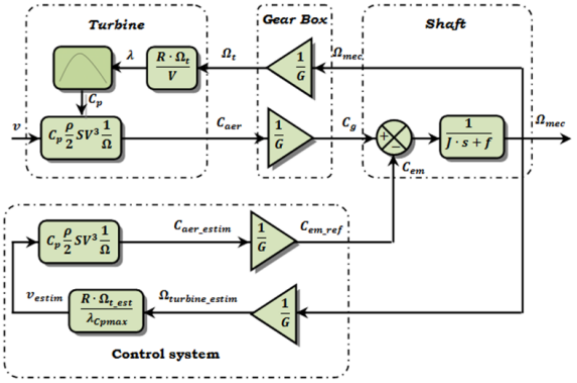

Fig. 4 Device control without control speed, [34].

The expression of the optimal mechanical power P_{mec_opt} is obtained as follows:

$$P_{mec_{opt}} = \frac{1}{2}\frac{C_{p_{max}} \cdot \rho \cdot \pi \cdot R^3}{G^3\lambda_{opt}^3} \cdot \Omega_{mec}^3 \quad (12)$$

3. Dynamical Model of the BDFIG

The electrical equations of the BDFIG in the synchronous reference frame (d-q) are this given by [6,7,12,18]:

$$v_{sp}^q = R_{sp}i_{sp}^q + \frac{d\psi_{sp}^q}{dt} + \omega_p\psi_{sp}^d \quad (13)$$

$$v_{sp}^d = R_{sp}i_{sp}^d + \frac{d\psi_{sp}^d}{dt} - \omega_p\psi_{sp}^q \quad (14)$$

$$0 = R_r i_r^q + \frac{d\psi_r^q}{dt} - (\omega_p - p_p\omega_r)\psi_r^d \quad (15)$$

$$0 = R_r i_r^d + \frac{d\psi_r^d}{dt} - (\omega_p - p_p\omega_r)\psi_r^q \quad (16)$$

$$v_{sc}^q = R_{sc}i_{sc}^q + \frac{d\psi_{sc}^q}{dt} + (\omega_p - (p_p + p_c)\omega_r)\psi_{sc}^d \quad (17)$$

$$v_{sc}^d = R_{sc}i_{sc}^d + \frac{d\psi_{sc}^d}{dt} + (\omega_p - (p_p + p_c)\omega_r)\psi_{sc}^q \quad (18)$$

The expressions for stator and rotor flux linkages are

$$\psi_{sp}^q = L_{sp}i_{sp}^q + L_{mp}i_r^q \quad (19)$$

$$\psi_{sp}^d = L_{sp}i_{sp}^d + L_{mp}i_r^d \quad (20)$$

$$\psi_r^q = L_{mp}i_{sp}^q + L_r i_r^q + L_{mc}i_{sc}^q \quad (21)$$

$$\psi_r^d = L_{mp}i_{sp}^d + L_r i_r^d + L_{mc}i_{sc}^d \quad (22)$$

$$\psi_{sc}^q = L_{sc}i_{sc}^q + L_{mc}i_r^q \quad (23)$$

$$\psi_{sc}^d = L_{sc}i_{sc}^d + L_{mc}i_r^d \quad (24)$$

The dynamic equations in (13-24) are usually represented in the selected d-q reference frame [12]. The general relationships between these quantities as well as the electrical speed of the rotor for the 50 Hz system are

$$\begin{cases} \omega_p = 2\pi \cdot 50 \\ \omega_r = \omega_p - \omega_r p_p \\ \omega_r = \omega_p - \omega_r(p_p + p_c) \end{cases} \quad (25)$$

The equation also shows the torque to be the function of the PW flux as well as the CW stator and rotor currents

$$C_{em} = \frac{3}{2}\left(p_p(\psi_{sp}^d i_{sp}^q - \psi_{sp}^q i_{sp}^d) + p_c L_{mc}(i_{sc}^d i_r^q - i_{sc}^q i_r^d)\right) \quad (26)$$

Finally, the mechanical model of BDFIG can be written as

$$J_g\frac{d\omega_m}{dt} = C_{em} - f_g\omega_m - C_L \quad (27)$$

The active and reactive power at the stator as well as those provide for grid are defined as

For PW are:

$$\begin{cases} P_p = \frac{3}{2}(v_{sp}^q\, i_{sp}^q + v_{sp}^d\, i_{sp}^d) \\ Q_p = \frac{3}{2}(v_{sp}^q\, i_{sp}^d + v_{sp}^d\, i_{sp}^q) \end{cases} \quad (28)$$

For CW are:

$$\begin{cases} P_c = \frac{3}{2}(v_{sp}^q\, i_{sp}^q + v_{sp}^d\, i_{sp}^d) \\ Q_c = \frac{3}{2}(v_{sc}^q\, i_{sc}^d + v_{sc}^d\, i_{sc}^q) \end{cases} \quad (29)$$

The active and reactive powers of the BDFIG are:

$$\begin{cases} P_T = P_p + P_c \\ Q_T = Q_p + Q_c \end{cases} \quad (30)$$

4. BDFIG Controller Design

4.1 Control of the grid inverter

The various control strategies for the voltage source rectifier (VSR) have been proposed [2,34] and will be briefly discussed here.

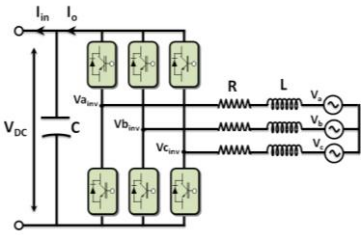

Fig. 5 VSR Circuit Model.

The objective of the grid inverter is to maintain a constant DC-link voltage between BDFIG (CW) and grid.

The system can be described by the following equation:

$$\begin{bmatrix} V_a \\ v_b \\ v_c \end{bmatrix} = R\begin{bmatrix} i_a \\ i_b \\ i_c \end{bmatrix} + L\frac{d}{dt}\begin{bmatrix} i_a \\ i_b \\ i_c \end{bmatrix} + \begin{bmatrix} V_{a_{inv}} \\ V_{b_{inv}} \\ V_{c_{inv}} \end{bmatrix} \quad (31)$$

This can be written in a rotating reference frame by using Park transformation

$$\begin{bmatrix} V_q \\ v_d \end{bmatrix} = R\begin{bmatrix} i_q \\ i_d \end{bmatrix} + L \cdot s\begin{bmatrix} i_q \\ i_d \end{bmatrix} + \omega_e L\begin{bmatrix} i_q \\ -i_d \end{bmatrix} + \begin{bmatrix} V_{q_{inv}} \\ V_{d_{inv}} \end{bmatrix} \quad (32)$$

Where s is the derivation operation.

$$\begin{cases} P = \frac{3}{2}\left(v_d i_d + v_q i_q\right) \\ Q = \frac{3}{2}\left(v_q i_d + v_d i_q\right) \end{cases} \quad (33)$$

The voltage components in the Park frame V_{d_inv} and V_{q_inv} are given at the output of the PI regulator:

$$\begin{cases} v_d^* = -i_d(s\,L + R) + \left(\omega_e\,L\,i_q + v_d\right) \\ v_q^* = -i_q(s\,L + R) + \left(\omega_e\,L\,i_d\right) \end{cases} \quad (34)$$

In the Park reference frame, the voltage source components are $V_d = 0$ and $V_q = V_s$ and the powers can be written as

$$\begin{cases} P = \frac{3}{2} v_q i_q \\ Q = \frac{3}{2} v_q i_d \end{cases} \quad (35)$$

By neglecting the converter losses, we have

$$\begin{cases} v_{dc} i_{dc} = \frac{3}{2} v_q i_q \\ C\frac{dv_{dc}}{dt} = i_{in} - i_o \end{cases} \quad (36)$$

$$v_{dc} C \frac{dv_{dc}}{dt} = P - P_m \quad (37)$$

The inner current loop can be modeled as a transfer function relating the terminal voltage and current

$$\frac{i(s)}{v(s)} = \frac{1}{L\,s + R} \quad (38)$$

The complete block diagram of the VSR controller is shown in Fig.6.

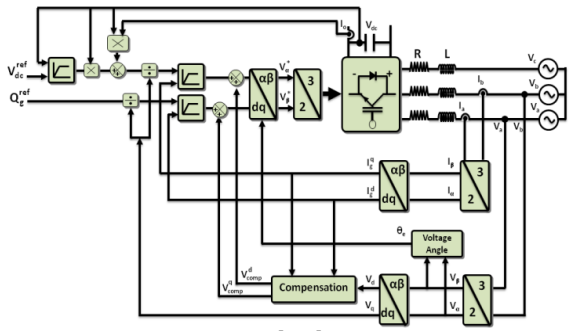

Fig. 6 Grid side VSR.

4.2 Power winding side Controller

4.2.1 Reference-frame

By choosing a reference frame linked to the PW flux, CW currents will be related directly to the PW active and reactive power. An adapted control of these currents will thus permit to control the power exchanged between the PW and the grid. If the PW flux is linked to the d-axis of the frame we have

$$\psi_p^d = \left|\psi_p\right| \text{ and } \psi_p^q = 0 \quad (39)$$

The obtained control strategy for the BDFIG is similar to the well-known stator field orientation control used in the DFIG.

4.2.2 Control strategy

By aligning the d-axes with the flux vector of the power winding allows for the further simplification of Eq. (28). Therefore, as in Eq. (40) the active power flow of the BDFIG can be regulated through the q-component of the PW current.

$$\left.\begin{aligned} P_p &= \frac{3}{2} v_{sp}^q\, i_{sp}^q \\ Q_p &= \frac{3}{2} v_{sp}^q\, i_{sp}^d \end{aligned}\right\} \quad (40)$$

The PW current can be expressed in terms of the rotor current and further CW stator current. Rearranging the PW stator flux and the rotor flux equations produces:

$$i_{sp} = \frac{\psi_{sp} - L_{mp} i_r}{L_{sp}} \quad (41)$$

$$i_r = \frac{\psi_r + L_{mp} i_r + L_{mc} i_{sc}}{L_r} \quad (42)$$

Then:

$$i_{sp} = \frac{L_r}{L_{sp}L_r - L_{mp}^2}\psi_{sp} - \frac{L_{mp}}{L_{sp}L_r - L_{mp}^2}\psi_r + \frac{L_{mc}L_{mp}}{L_{sp}L_r - L_{mp}^2} i_{sc} \quad (43)$$

Expanding Eq. (43) into d-q reference frame and substituting into Eq. (40) produces the expanded power flow expression for the BDFIG:

$$\begin{cases} P_p = \frac{3}{2} v_{sp}^q \left(\frac{L_{mp}}{L_{sp}L_r - L_{mp}^2}\psi_r^q - \frac{L_{mc}L_{mp}}{L_{sp}L_r - L_{mp}^2} i_{sc}^q\right) \\ Q_p = \frac{3}{2} v_{sp}^q \left(\frac{L_r}{L_{sp}L_r - L_{mp}^2}\psi_{sp}^d - \frac{L_{mp}}{L_{sp}L_r - L_{mp}^2}\psi_r^d + \frac{L_{mc}L_{mp}}{L_{sp}L_r - L_{mp}^2} i_{sc}^d\right) \end{cases} \quad (44)$$

The power terms in Eq. (44) are both expressed as a function of the CW stator current that can be directly controlled.

To begin the implementation of the power flow equations Eq. (44) in the controller, it is first necessary to trace the relationship between the current control signals of the CW and their equivalent voltage commands that can be utilized with the voltage source inverter:

$$v_{sc} = R_{sp}\, i_{sc} + \frac{d\psi_{sc}}{dt} + j\omega_c \psi_{sc} \quad (45)$$

The CW stator flux is estimated in Eq. (46). Rearranging the CW stator flux and expressing it in terms of some known quantities as well as rotor flux:

$$\psi_{sc} = \frac{L_{mc}L_{mp}}{L_r} i_{sp} - \frac{L_{mc}}{L_r}\psi_r + \frac{L_{sp}L_r - L_{mp}^2}{L_r} i_{sc} \quad (46)$$

For further simplification Eq. (43) can be substituted into Eq. (46), the result is then put into Eq. (45) and transformed into d-q frame:

$$\begin{cases} v_{sc}^d = R_{sc} i_{sc}^d + \frac{d}{dt}\left(\delta_3 i_{sc}^d + \delta_2 \psi_r^d - \delta_1 \psi_{sp}^d\right) - \omega_c\left(\delta_3 i_{sc}^q + \delta_3 \psi_r^q\right) \\ v_{sc}^q = R_{sc} i_{sc}^q + \frac{d}{dt}\left(\delta_3 i_{sc}^q + \delta_2 \psi_r^q\right) - \omega_c\left(\delta_3 i_{sc}^d + \delta_2 \psi_r^d - \delta_1 \psi_{sp}^d\right) \end{cases} \quad (47)$$

Thus, voltage expressions in Eq.(47) become the command signals to the controller of the VSI converter, shown in Fig.7. All the terms in Eq. (47) in square brackets represent the disturbance terms due to the various cross-coupling effects between the d-q components as well as the rotor cross-coupling. The leakages factors associated with these disturbances are:

$$\delta_1 = \frac{L_{mc}L_{mp}}{L_r L_{sp} - L_{mp}^2};\ \delta_2 = \frac{L_{mc}L_{sp}}{L_r L_{sp} - L_{mp}^2};\ \delta_3 = L_{sc} - \frac{L_{mc}^2 L_{sp}}{L_r L_{sp} - L_{mp}^2} \quad (48)$$

The disturbance associated with the derivative terms in Eq. (47) does not need to be included into the model because the controllers will be able to suppress them.

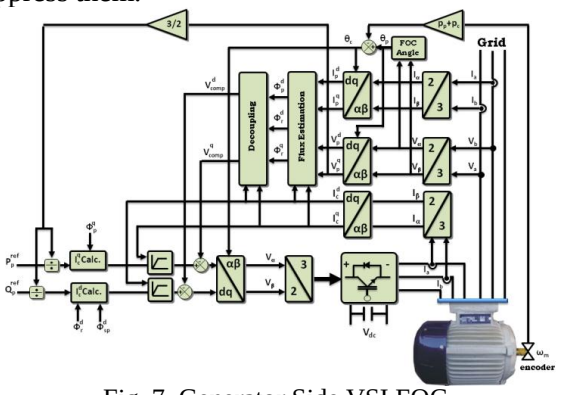

Fig. 7. Generator Side VSI FOC.

In the Eq. (47) is the presence of the PW stator flux and the rotor flux in as the control variables. We can't be measured directly of these quantities and would have to be estimated from the available voltage and current signals.

The reference frame is aligned with the d-component of the ψ_{sp}, the q-component (ψ_{sp}^{q}) always remains at zero. The d-component of the PW stator flux is then calculated as:

$$\psi_{sp}^{d} = \frac{V_{sp}^{q}}{2\pi 50} \quad (49)$$

The rotor flux estimations are based on the knowledge of the power and control machine currents as well as power machine flux in Eq.(45). By combining rotor flux expressions in Eq. 16-19 gives the estimated rotor flux in d-q reference frame:

$$\psi_r^q = \frac{L_{mp}^2 - L_{sp}L_r}{L_{mp}} i_{sp}^q + L_{mc} i_{sc}^q \quad (50)$$

$$\psi_r^d = \frac{L_{mp}^2 - L_r L_{sp}}{L_{mp}} i_{sp}^d + \frac{L_r}{L_{mp}} \psi_{sp}^d + L_{mc} i_{sc}^d \quad (51)$$

The structure of the VSI controller allows for the outer speed control loop producing the required reference current signal i_{sc}^{q}. The i_{sc}^{d} reference signal can be obtained directly from the desired reactive power command by applying Eq.(52) to it.

$$i_{sc_{ref}}^{d} = \frac{P_{p_{ref}}}{1.5\, v_{sp}\, \delta_1} + \frac{\delta_4}{\delta_1}\psi_r^q \quad (52)$$

$$i_{sc_{ref}}^{q} = \frac{Q_{p_{ref}}}{1.5\, v_{sp}\, \delta_1} - \frac{\delta_5}{\delta_1}\psi_{sp}^d + \frac{\delta_4}{\delta_1}\psi_r^d \quad (53)$$

Where

$$\delta_4 = \frac{L_{mp}}{L_r L_{sp} - L_{mp}^2}, \delta_5 = \frac{L_r}{L_r L_{sp} - L_{mp}^2} \quad (54)$$

5. Controllers synthesis

In this section, we have chosen to compare the performances of the BDFIG with two different controllers.

5.1 PID controller synthesis

At present, the PID-type controller is most widely adopted in industrial application due to its simple structure, as shown Fig. 8. Its control signal is easily computed by combining proportional-integral-Derivative terms, weighted according to the independent gain parameters P, I, and D [35]. The filter coefficient N sets the location of the pole in the derivative filter.

The control signal is

$$u(t) = \left[K_p + K_i\left(\frac{1}{s}\right) + K_d\left(\frac{N\,s}{s+N}\right)\right] e(t) \quad (55)$$

Where K_p, K_i and K_d are the PID controller parameters.

The quotient B/A represents the transfer function to be controlled, where A and B are presently defined as follows:

$$A = R_{sc} + s\,\delta_3 \text{ and } B = 1 \quad (56)$$

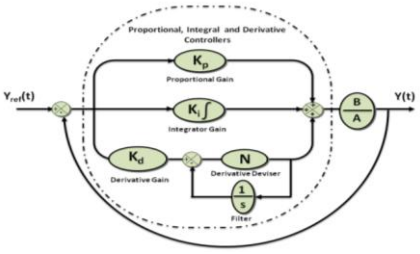

Fig. 8. System with PID controller.

The controller terms can be calculated just specifying the natural frequency and damping of the close loop equivalent second order system. The desired natural frequency (ω_n) and damping (ξ) are set respectively to 37 rad/s and 70.7 %.

Allows determining the parameters of PID controller:

K_p = 1.84, K_i = 62, K_d = 0.015 and N = 123.

5.2 Fuzzy P+ID controller synthesis

In this section, we would like to keep the advantages of the PID controller while designing a fuzzy logic controller. This idea leads to propose a hybrid fuzzy P+ID controller shown in Fig. 9. This hybrid controller uses an incremental fuzzy logic controller in place of the proportional term while the integral and derivative terms keep unchanged

$$u(t) = \left[K_p u_f(t) + K_i\left(\frac{1}{s}\right) + K_d\left(\frac{N\,s}{s+N}\right)\right] e(t) \quad (57)$$

Where K_i and K_d are identical to the conventional PID controller, is the output of the incremental fuzzy logic controller, and K_p is its proportional coefficient. The most important part in the fuzzy P+ID controller is the fuzzy K_p term because it is responsible for improving overshoot and rise time. The conventional K_i term is mainly responsible for reducing a steady-state error if an actual value is close to a reference signal. The conventional K_d term is responsible for the stability of the system and for the flatness of the response [26,27,28,29,30,35], The

filter coefficient N sets the location of the pole in the derivative filter.

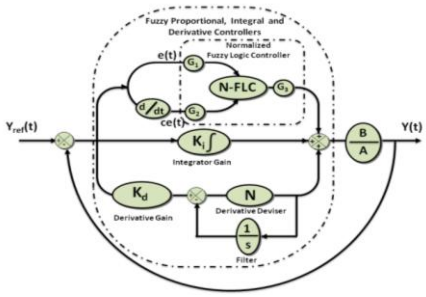

Fig. 10 System with Fuzzy P+ID controller.

Fig. 10 shows block diagram of a Fuzzy logic controller (FLC). It consists of fuzzification; inference mechanism, knowledge base and a defuzzification block [31,32,33,36]. In this proposed FLC the variables linguistic input are the current error e (t) and rate of change of current error ce(t) and the variable linguistic output is the current producing voltage component.

$$e(t) = i_{sc}^{*}(t_s) - i_{sc}(t_s) \quad (58)$$

$$ce(t_s) = e(t_s) - e(t_s - 1) \quad (59)$$

Where $i_{sc}(ts)$ is the actual stator current of CW and $i_{sc}^{*}(t_s)$ is the reference stator current of CW at current sampling time ts, e(ts-1) is the error at previous sampling time, $e(t_s)$ is the current error at current sampling time ts. The inputs and the output are related as:

$$u_f(t_s) = f\big(e(t_s), ce(t_s)\big) \quad (60)$$

The fuzzy logic controller is a standard one which has two inputs e(t) and ce(t) and an output uf(t). The scaling factors G1, G2 and G3 are chosen for normalization. The factors G1 and G2 are used to normalized error e(t) and change of error ce(t)respectively, so that these remain within the limit of -1 to +1. This process of converting crisp variables into fuzzy variables is called fuzzification. After selecting the scaling factors, the next step is to choose the membership function for e(t), ce(t) and uf(t). The membership functions used for the input and output fuzzy set are shown in Fig. 11. Here triangular membership functions are used and labeled as: Z=Zero, PS=Positive small, PM=Positive Medium, PB=Positive Big, NS=Negative Small, NM=Negative Medium, NB= Negative Big, PVS=Positive Very small and NVS= Negative Very Small. All the membership functions have asymmetrical shape with more crowding near the origin for higher precision at steady state.

The knowledge base involves defining the rules represented as IF -THEN rules statements governing the relationship between inputs and output variables in terms of membership functions. In this stage the input variables e and ce are processed by the inference engine that executes 7×7 rules shown in rule Tab. 1. A typical rule can be written as follows.

If e is ak and ce is bk then output is ck

Where ak , bk, ck are the labels of linguistic variables of error (e), change of error (ce) and output (uf) respectively.

Inferencing mechanism includes application of fuzzy operator AND (∩), OR (U) and NOT (-).

AND → Intersection: $\mu a \cap b = \min[\mu a(x), \mu b(x)]$

OR → Union: $\mu a \cup b = \max[\mu a(x), \mu b(x)]$

NOT → Complement: $\mu a = 1 - \mu a(x)$

After processing the inputs through knowledge base and inferencing mechanism the next stage is defuzzification. In this stage the fuzzy variables are converted into a crisp variable [31,32,33,36]. This stage introduces different inference methods that can be used to produce the fuzzy set value for the output fuzzy variable uf. In this, the center of gravity or centroid method is used to calculate the final fuzzy value uf [32]. The output function is given as:

$$u_f = \frac{\sum_{k=1}^{n} u_{f(k)} \cdot \mu\big(u_{f(k)}\big)}{\sum_{k=1}^{n} \mu\big(u_{f(k)}\big)} \quad (61)$$

Where n is the total number of rules and $\mu(u_f(k))$ denotes the output membership value for k^{th} rule.

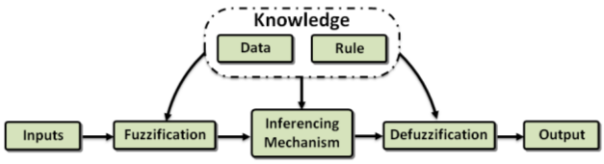

Fig. 11 Block diagram of fuzzy controller.

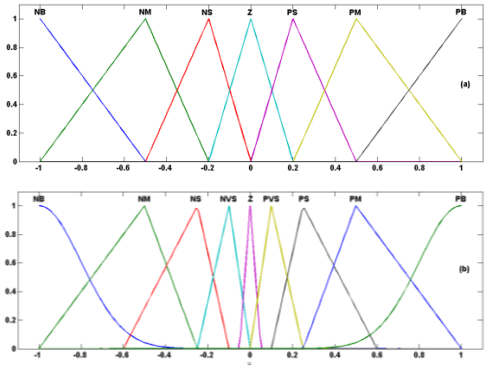

Fig. 12 Membership functions for: (a) error e and change of error ce and (b) output uf.

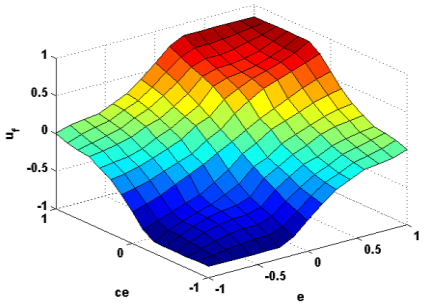

Fig. 13 Control surface of the fuzzy logic controller.

ce \ e	NB	NM	NS	Z	PS	PM	PB
NB	NB	NB	NB	NM	NS	NV	Z
NM	NB	NM	NM	NS	NV	Z	PV
NS	NB	NM	NS	NV	Z	PV	PS
Z	NM	NS	NV	Z	PV	PS	PM
PS	NS	NV	Z	PV	PS	PM	PB
PM	NV	Z	PV	PS	PM	PM	PB
PB	Z	PV	PS	PM	PB	PB	PB

Table 1 Fuzzy rule base of the fuzzy logic controller.

6. Simulation Results And Discussion

The aim of the control is to measure active and reactive powers equal to the reference values. These powers must then be collected. In order to measure only the stator current of CW. The two controllers have been tested using the indirect control method. The indirect control mode is based on the stator currents measurements of CW,

The indirect control mode is based on the stator currents measurements of CW and gives then best results for the DFIG control (in spite of small static error), in order to minimize the number and complexity of the presented results.

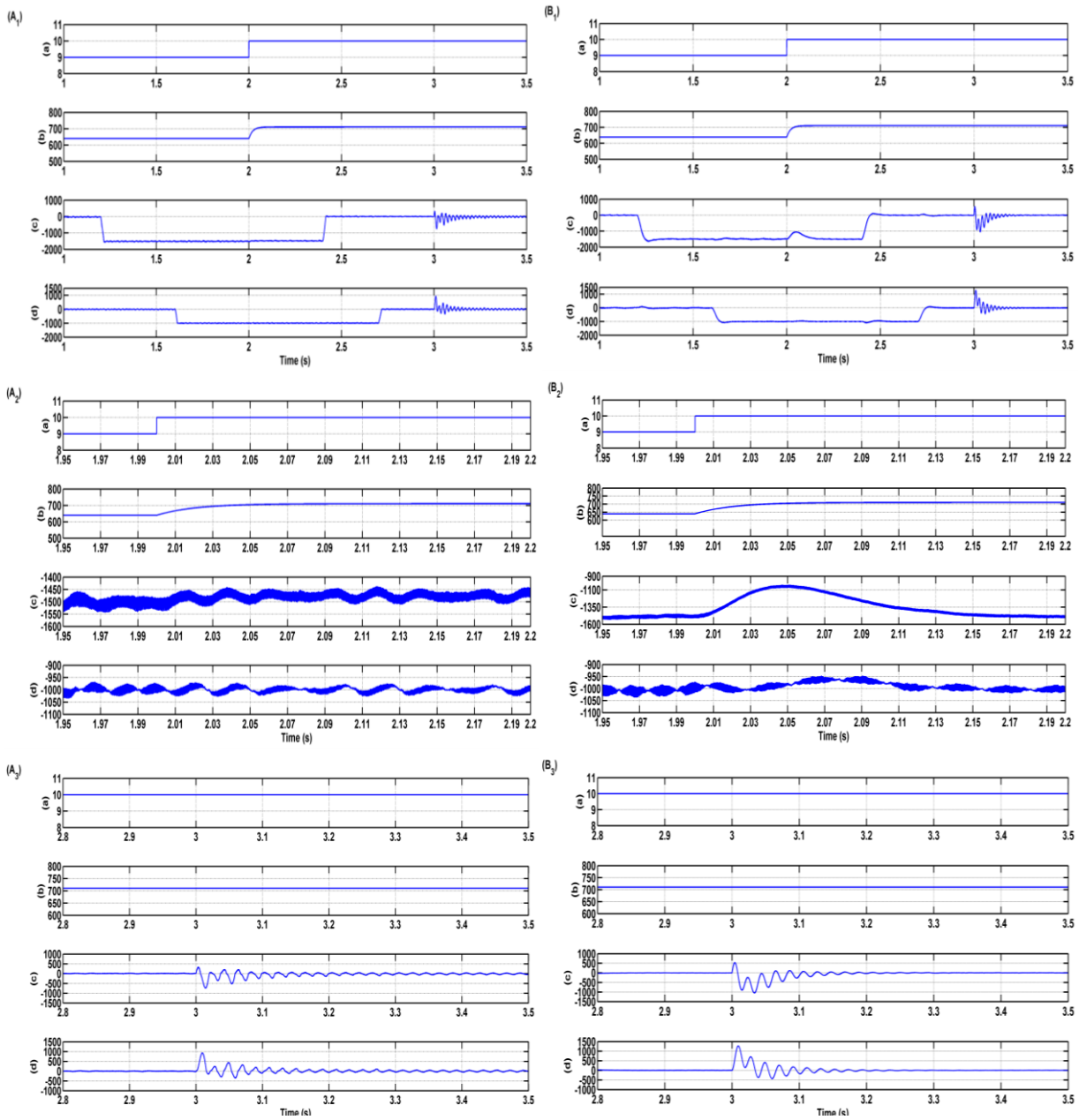

Fig. 14. Simulated results under various speed, stator reactive power steps and parameters variation.
(A) Fuzzy P+ID controller. (B) PID controller.
(1) Reference tracking. (2) Effect of a speed variation. (3) Effect of machine's parameters variation.
(a) Wind speed (m/s). (b) Rotor speed (rd/s). (c) Stator active power of PW (W). (d) Stator reactive power of PW (Var).

6.1 Performances of the controller

6.1.1 Reference tracking

The first test investigated to compare the both controllers is reference tracking by applying stator active and reactive power steps of PW, respectively. As shown in Fig. 14, the active power is stepped from 0 to -1.5 kW (export to grid) at 1.2 s and then backed to 0 at 2.4 s, the reactive power is stepped from 0 to -1 kW at 1.6 s and then backed to 0 at 2.7 s, while the machine's speed is maintained constant during the first change at 640 rd/s and at 710 rd/s during the second change. The results are presented in Fig. 14A1 and Fig. 14B1.

The Fig.14B1 shown during the change of power, transient oscillations due to the coupling terms between the two axes and static error appear on active and reactive powers. This is inherent to the adopted control mode: the feedback signal of the controller is calculated using stator currents of CW and considering that stator resistance of CW is neglected. It can be seen that transient oscillations amplitude are minimized with Fuzzy P+ID controller which have better rejection of perturbations. Therefore we can consider that the both controllers have almost equivalent behaviour for this test.

6.1.2 Sensibility to perturbations

The aim of this test is to analyze the influence of a speed variation of the BDFIG on active and reactive powers. The active and reactive power references are maintained to −1.5 kW and -1 kVAR and at time equal to 2 s the speed varies from 640 rd/s to 710 rd/s. The results are shown in Fig. 14A2 and 14B2.

This figure shows the limits of the PID controller. Indeed, for this controller, a speed variation induces an important variation of the active and reactive powers (18% for active power and 2% for reactive power). The Fuzzy P+ID controller has a nearly perfect speed disturbance rejection, indeed, only small power variations can be observed (less than 1% for active power and 0.5% for reactive power). This result is interesting for wind energy applications to ensure stability and quality of the generated power when the speed is varying.

6.1.3 Robustness

The aim of this test is to analyze the influence of the BDFIG's parameters variations on the controller's performances. The machine's model parameters have been deliberately modified with excessive variations: the values of the both stators and the rotor resistances are increased by 25% and the values of inductances are reduced by 25%. The BDFIG is running at 710 rd/s, active and reactive powers are maintained constant and the speed is equal to 710 rd/s. The obtained results are presented in Fig. 14A3 and 14B3.

These results show that parameters variations of the BDFIG increase the time-response of the PID and Fuzzy P+ID controllers, for the PID controller, parameters variations induces an important variation of the active and reactive powers (40% for active power and 50% for reactive power), and Fuzzy P+ID controller have lower than the previous values (28% for active power and 36% for reactive power). Indeed, the transient oscillations due to the coupling terms between the two axes are always present for all controllers but their amplitudes have not been increased compared to the test with no parameters variation. However, a static error on reactive power appears when the value of the active power is changed but it keeps reasonable values

1.1 Simulation of the whole system

The brushless doubly fed induction generator parameters used in the simulation are given as following:

Table 2. BDFIG Parameters used for Simulation

Turbine	Diameter = 4.6 m, Number of blades = 3, Hub height = 12 m, Gearbox = 18
BDFIG	2.5 Kw, 380 V, 50 Hz, 2 pole pairs, R_{sp} = 1.732 Ω, R_{sc} = 1.079 Ω, R_r = 0.473Ω, L_{sp} = 714.8 mH, L_{sc} = 121.7 mH, L_r = 132.6 mH.
Grid	U = 380 V, Zline =R +jLω = 0.25 +j0.003.

Fig. 15 shows the wind speed. Fig. 16 shows the angular speed random of the BDFIG. Fig. 17 presents the wind generator mechanical power. Fig. 18 shows the random form of the generator torque. The decoupling effect between the direct and quadratic stator flux of PW is illustrated in Fig. 19. The stator currents and voltages waveforms of the BDFIG and the related expended plots are shown, respectively, in Fig. 20a, Fig. 20b, Fig. 20c and Fig. 20d (phase *a*). The PWM inverters are operated at 2 kHz; hence, the currents are almost sinusoidal. The stator currents (PW and CW) waveforms and these zoom are presented, correspondingly, in Fig. 21a and Fig. 21b. Fig. 22 gives the rotor current of the BDFIG. The grid voltage and current waveforms and these zoom are presented, correspondingly, in Fig. 23a and Fig. 23b. The stator active and reactive powers are plotted in Fig. 24. Fig. 25a and Fig. 25b show the regulation of the DC-link voltage. It is

maintained at a constant level (410 V) so that the real power extracted from the wind energy conversion system can pass through the grid.

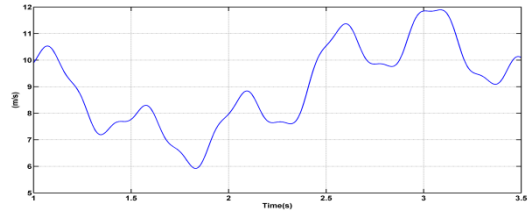

Fig. 15 wind speed (V_w).

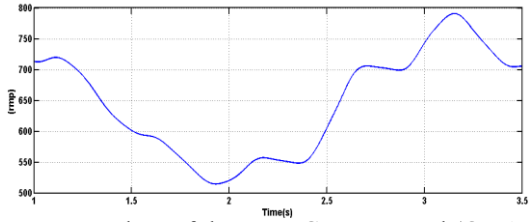

Fig. 16 Random of the BDFIG rotor speed (Ω_{mec}).

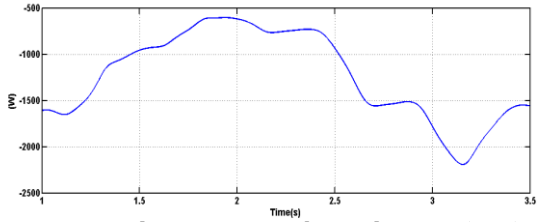

Fig. 17 Wind generator mechanical power (P_{mec}).

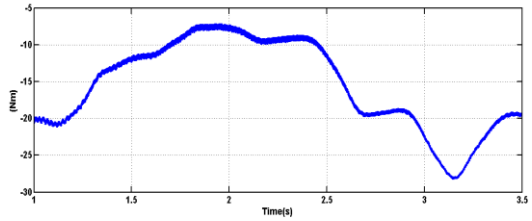

Fig. 18 Generator torque (T_{em}).

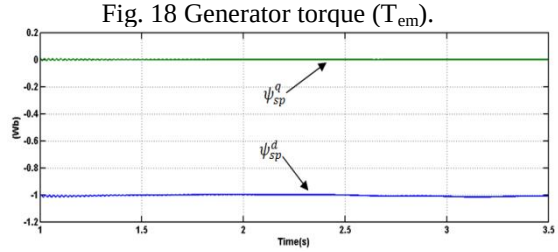

Fig. 19 Direct and quadratic stator flux of PW (ψ_{sp}^{q} and ψ_{sp}^{d}).

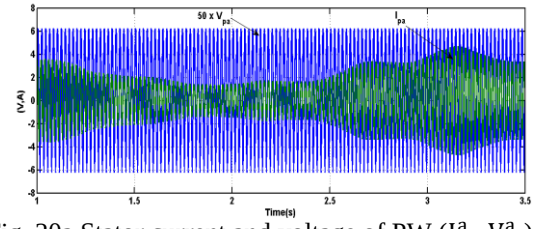

Fig. 20a Stator current and voltage of PW (I_{sp}^{a}, V_{sp}^{a}).

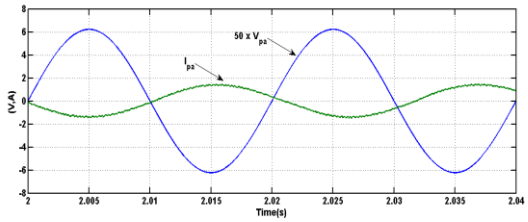

Fig. 21b Zoom of Stator current and voltage of PW (I_{sp}^{a}, V_{sp}^{a}).

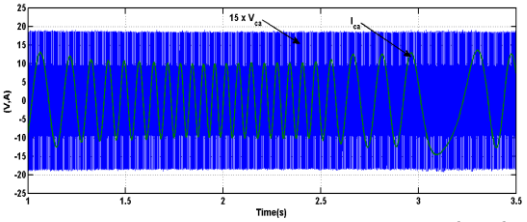

Fig. 21c Stator current and voltage of CW (I_{sc}^{a}, V_{sc}^{a}).

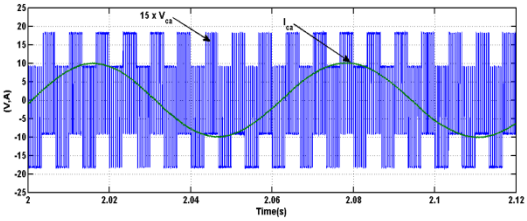

Fig. 21d Zoom of Stator current and voltage of CW (I_{sc}^{a}, V_{sc}^{a}).

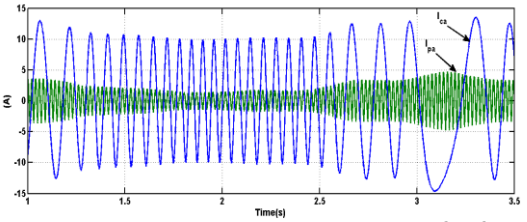

Fig. 22a Stator currents of PW and CW (I_{sc}^{a}, I_{sp}^{a}).

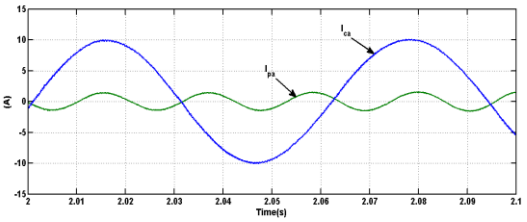

Fig. 22b Zoom of Stator currents of PW and CW (I_{sc}^{a}, I_{sp}^{a}).

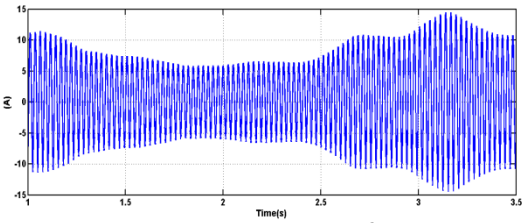

Fig. 25 Rotor current (I_{r}^{a}).

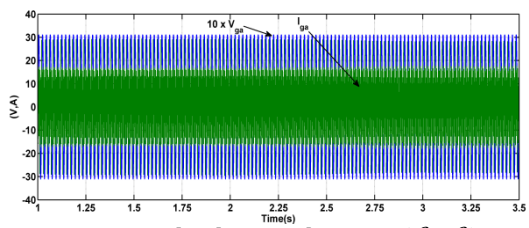

Fig. 23a Grid voltage and current (I_{g}^{a}, V_{g}^{a}).

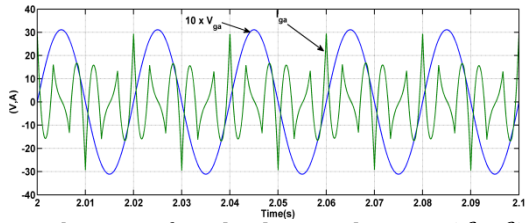

Fig. 23b Zoom of Grid voltage and current (I_g^a, V_g^a).

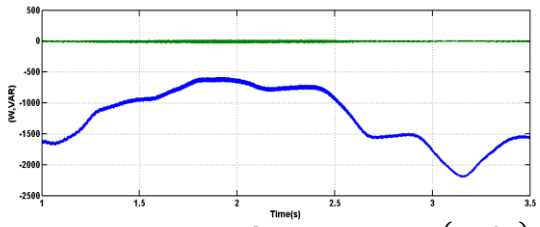

Fig. 24 Stator active and reactive powers (P_p, Q_p).

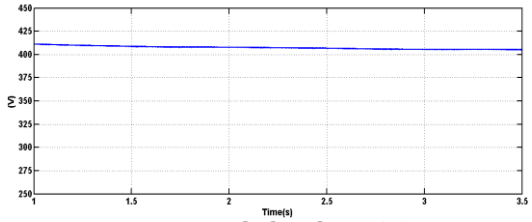

Fig. 25a DC-link voltage (E).

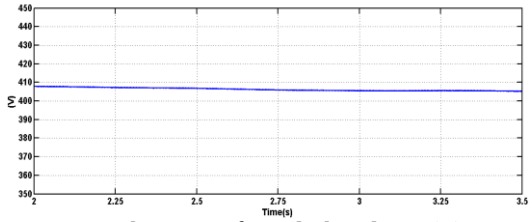

Fig. 25b Zoom of DC-link voltage (E)

2. Conclusions

In this paper a fuzzy logic proportional controller and a conventional integral and derivative (Fuzzy P+ID) control associated to the oriented control field of a brushless doubly fed induction generator based wind energy conversion systems connected to the grid has been presented. The structure of the Fuzzy P+ID controller is very simple since it is constructed by replacing the proportional term in the conventional PID controller with an incremental fuzzy logic controller [26,27,28].

In this paper, we have presented a complete system to produce electrical energy with a BDFIG by the way of a wind turbine. Two different controllers are synthesized and compared. In term of power reference tracking with the BDFIG in ideal conditions (no parameters variations and no disturbances), the performances of the two controllers are similar. When the machine's speed is modified (which represents a perturbation for the system), the impact on the active and reactive powers values is important for PID whereas it is almost non-existent for Fuzzy P+ID.

A robustness test has also been investigated where the machine's parameters have been modified. These changes induce time-response variations with PID and Fuzzy P+ID controllers. The static error on the reactive power appears when the active power is modified but it is due to the indirect control mode and it can be numerically compensated in future works.

The grid inverter has also been controlled with a PI controller in order to maintain the DC-bus voltage to a constant value. A test has been investigated with speed, active and reactive power variations showing negligible variations of the voltage. The last part of the paper shows the possibility to simulate the whole system behavior with a turbine. The presented results show that intelligent control method as Fuzzy P+ID can be a very attractive solution for devices using BDFIG such as wind energy conversion systems. Indeed, most of the studied BDFIG control schemes use classical PID controllers but the comparison done in this paper show that the limits of this type of controller can have negative effects on the quality and the quantity of the generated power.

Appendix A. Nomenclature

The turbine

Ω_{mec}	Mechanical speed of the BDFIG
Ω_t	Turbine speed
Ω_{mec_ref}	Mechanical speed reference
P_t	Mechanical power
P_{mec_ref}	Mechanical power optimal
C_{aer}	Aerodynamic torque
C_g	Generator torque
C_p	Power coefficient
Λ	Tip speed ratio
P	Air density
R	Turbine radius
V_w	Wind velocity
G	Gear ratio
S	cross-sectional area
J_t	Inertia
F_t	Viscous friction

The BDFIG

$V_{sp}^q, V_{sp}^d, V_{sc}^q, V_{sc}^d,$	"d-q" stators voltages
$i_{sp}^q, i_{sp}^d, i_{sc}^q, i_{sc}^d$	"d-q" stators currents
$\psi_{sp}^q, \psi_{sp}^d, \psi_{sc}^q, \psi_{sc}^d$	"d-q" stators flux
V_r^q, V_r^d	"d-q" rotor voltages
i_r^q, i_r^d	"d-q" rotor currents

N_r	Number of rotor nests
R_{sp}, R_{sc}	Per phase stators resistances
R_r	Per phase rotor resistance
L_{sp}, L_{sc}	Total cyclic stators inductances
L_r	Total cyclic rotor inductance
L_{mp},L_{mc}	Magnetizing inductances
P	Number of pole pairs
S	derivative operator
J_g	inertia
F_g	viscous friction
C_{em}	electromagnetic torque
P_p, Q_p	active and reactive stator powers
P_g, Q_g	active and reactive grid powers
ω_e	speed of the reference frame
ω_p, ω_c,	stators synchronous angular frequency
ω_r	rotor's electrical angular speed
ω_m	rotor's mechanical angular speed

3. References

[1] Kostyantyn Protsenko, Dewei Xu, Modeling and control of brushless doubly fed induction generators in wind energy applications, IEEE Trans. Pow. Elec., Vol. 23, No.3, (2008) 1191-1197.

[2] Kostyantyn Protsenko, Dewei Xu, Modeling and control of brushless doubly fed induction generators in wind energy applications, APEC, (2007) 529 – 535.

[3] Heng Niana, Yu Quana, Jiabing Hub, improved control strategy of DFIG-based wind power generation systems connected to a harmonically polluted network, EPSR Elsevier, Volume 86 (2012) 84–97.

[4] H. Amimeur, D. Aouzellag, R. Abdessemed, K. Ghedamsi, Sliding mode control of a dual-stator induction generator for wind energy conversion systems, IJEP Elsevier, Vol. 42, no. 1, (2012) 60–70.

[5] E. Abdi, X. Wang, Sh. Shao and R. McMahon, Performance Characterization of Brushless Doubly-Fed Generator, IAS '08, (2008) 1-6.

[6] J. Poza, E. Oyarbide, I. Sarasola, M. Rodriguez Unified reference frame dq model of the brushless doubly fed machine, IEE Proc. Electr. Power Appl., Vol. 153, No. 5, (2006) 726-734.

[7] Janvier Poza, Estanis Oyarbide, Daniel Roye, New vector control algorithm for brushless doubly fed machines, IECON'02 Conference, Spain (2002) 1138-1143.

[8] H. Oraee, E. Abdi,S. Shao,R. McMahon, The Brushless Doubly-Fed Machine Vector Model in the Rotor Flux Oriented Reference Frame, IECON'08 (2008) 1415 – 1420.

[9] Ardiaty Ariefa, ZhaoYang Dongb, Muhammad Bachtiar Nappua, Marcus Gallagherc, Under voltage load shedding in power systems with wind turbine-driven doubly fed induction generators, EPSR Elsevier, Volume 96, (2013) 91–100.

[10] Mohammad Verij Kazemia, Morteza Moradib, Reza Verij Kazemic, Minimization of powers ripple of direct power controlled DFIG by fuzzy controller and improved discrete space vector modulation, EPSR Elsevier, Volume 89 (2012) 23–30.

[11] Dan Levy, Stand alone induction generators, EPSR Elsevier, Volume 41, Issue 3, (1997), 191–201

[12] J. Poza, E. Oyarbide, I. Sarasola, M. Rodriguez, Vector control design and experimental evaluation for the brushless doubly fed machine, IET Electr. Power Appl, Vol. 3, Iss. 4, (2009) 247–256.

[13] F. Poitiers, T. Bouaouiche, M. Machmoum, Advanced control of a doubly-fed induction generator for wind energy conversion, EPSR Elsevier, Vol.79, no 7, (2009) 1085-1096.

[14] F. Runcos, R. Carlson, A. Oliveira, P. Kuo-Pen, N. Sadowski, Performance Analysis of a Brushless Double Fed Cage Induction Generator, Proc. Nordic Wind Power Conference (2004) 1- 8.

[15] P J Tavner, R A McMahon, P Roberts, E Abdi-Jalebi, X Wang, M Jagieła, T Chick, Rotor Design & Performance for a BDFM, ICEM Greece (2006)

[16] P.C. Roberts, R.A. McMahon, P.J. Tavner, J.M. Maciejowski, T.J. Flack, X. Wang, Performance of Rotors in a Brushless Doubly-Fed Induction Machine (BDFM), ICEM, Poland, 2004.

[17] Wallace A.K., Spee, R., Alexander, G.C. The brushless doubly-fed machine: its advantages, applications and design methods, 6th Inte. Conf. on EMD, (1993) 511 – 517.

[18] Izaskun Sarasola, Javier Poza, Miguel A. Rodriguez, Gonzalo Abad, Direct torque control design and experimental evaluation for the brushless doubly fed machine, ECM, Vol. 52, no. 2, (2011) 1226-1234.

[19] Shiyi Shao; Abdi, E.; McMahon, R, Low-Cost Variable Speed Drive Based on a Brushless Doubly-fed Motor and a Fractional Unidirectional Converter, IEEE Trans. Ind. Elec., Vol. 59 , no. 1 (2012) 317 – 325.

[20] F. Blazquez, C. Veganzones, D. Ramırez, C. Platero, Characterization of the Rotor Magnetic Fieldin a Brushless Doubly-Fed Induction Machine, IEEE Trans. Ener. Conv., VOL. 24, NO. 3 (2009) 599 – 607.

[21] D. Picovici, D. Levy, A.E. Mahdi, T. Coffey, The cascade induction machine: a reliable and controllable motor or generator, Volume 68, Issue 3 (2004) 193–207.

[22] Shiyi Shao, Abdi, E., Barati, F., McMahon, R, Stator-Flux-Oriented Vector Control for Brushless Doubly Fed Induction Generator, IEEE Trans. Ind. Electro., Vol. 56, no. 10 (2009) 4220 – 4228.

[23] Paul C. Roberts, A Study of Brushless Doubly-Fed

(Induction) Machines, Thesis of PhD, University of Cambridge, 2004.
[24] Sh. Shao, T. Long, E. Abdi , R. McMahon, Dynamic Control of the Brushless Doubly Fed Induction Generator Under Unbalanced Operation, IEEE Trans. Ind. Electro., Issue 99 (2012).
[25] Sh. Shao, T. Long, E. Abdi, R. McMahon, W. Yunxiang, Symmetrical Low Voltage Ride-Through of the Brushless Doubly-Fed Induction Generator, IECON (2011) 3209 – 3214.
[26] W. Li, X.G. Chang, F.M. Wahl, Jay Farrell, Technical note Hybrid fuzzy P+ID control of manipulators under uncertainty, Mechatronics, Vol. 9, Issue 3 (1999) 301–315.
[27] W. Lia, X.G. Changa, F.M. Wahlb, Jay Farrellc, Tracking control of a manipulator under uncertainty by FUZZY P+ID controller, FSS Elsevier, Vol. 122, Issue 1 (2001) 125–137.
[28] Wei Li, Design of a Hybrid Fuzzy Logic Proportional Plus Conventional Integral-Derivative Controller" IEEE Trans. Fuz. Sys., Vol. 6, No. 4 (1998) 449 – 463.
[29] Wei Li, Xiaoguang Chang, Application of hybrid fuzzy logic proportional plus conventional integral-derivative controller to combustion control of stoker-fired boilers, FSS Elsevier, Vol. 111, Issue 2, (2000) 267–284.
[30] Dave Misir, Heidar A. Malki, Guanrong Chen, Design and analysis of a fuzzy proportional-integral-derivative controller Original Research Article, FSS Elsevier, Vol. 79, Issue 3 (1996) 297-314.
[31] L. A. Zadeh, Fuzzy Sets, IC Elsevier, Vol. 8 (1965) 338-353.
[32] Benudhar Sahu, K.B.Mohanty, Swagat Pati, A Comparative Study on Fuzzy and PI Speed Controllers for Field-Oriented Induction Motor Drive, MEPS'10 (2010) 7-14.
[33] Jae-Sung Yu, Sang-Hoon Kim, Byoung-Kuk Lee, Chung-Yuen Won, Jin Hur, Fuzzy-Logic-Based Vector Control Scheme for Permanent-Magnet Synchronous Motors in Elevator Drive Applications, IEEE Trans. Indus. elect., vol. 54, no. 4 (2007) 2190 – 2200.
[34] R. Pena, J.C.Clare, G. M. Asher, Doubly fed induction generator uising back-to-back PWM converters and its application to variable speed wind-energy generation, IEE Proc. Electr. Pow. Appl., Vol. 143, No 3 (1996) 231 – 241.
[35] K. Astrom, T. Hagglund, PID Controllers : Theory, Design, and Tuning", Inst. Society of America, 1995.
[36] Lamchich, M.T., Raoufi, M.: A Fuzzy Logic based Controller for Shunt Active Power Filter, Journal of Electrical Engineering vol.8,2008.